Pergamon

Journal of Structural Geology, Vol. 17, No. 11, pp. 1615 to 1620, 1995

0191-8141/95 $9.50+0.00

0191-8141(95)E0016-E

Deflection of pure shear viscous flow around a rigid spherical body

TOSHIAKI MASUDA* and NAOYA MIZUNO†

Institute of Geosciences, Shizuoka University, Shizuoka 442, Japan

(*Received* 6 *October* 1994; *accepted in revised form* 24 *April* 1995)

Abstract—This paper theoretically simulates viscous flow around a rigid spherical body during far-field pure shear deformation, and derives the velocity vector, kinematical parameters such as the rate-of-strain tensor and dynamic parameters such as the differential stress. The results are applied to microstructures around porphyroblasts and porphyroclasts. They reveal that in the pressure shadow regions pressure is lower, but differential stress is rather higher, and the strain is larger. Thus, this region is not a 'shadow' region for deformation.

INTRODUCTION

Pure shear deformation of a homogeneous material is one of the fundamental deformation modes which is analysed in textbooks of structural geology (e.g. Jaeger & Cook 1969, Means 1976, Ramsay & Huber 1983). However, if a rigid spherical body is enclosed in a material in pure shear, the deformation will be highly disturbed around the sphere. Locally, the deformation is no longer perfect pure shear. This paper deals with such deformation in theory, and will quantify particle paths, kinematic parameters such as the rate-of-strain tensor, and dynamic parameters such as the stress tensor anywhere in the matrix around a rigid sphere. Some results are already established by Oertel (1965). However, Oertel's analysis is restricted to a narrow region close to the sphere. The present paper will analyse more parameters relevant to geological structures, and in a wider region than Oertel's (1965). The analysis simulates deformation around porphyroclasts, porphyroblasts or pebbles. This paper specially discusses physical conditions in 'pressure shadow regions' around a porphyroblast in metamorphic rocks.

METHOD

We assume that the viscous material is an incompressible Newtonian fluid and that the deformation is very slow and not time-dependent. A rigid sphere of unit radius is embedded in the fluid so that its centre is situated at the origin of the Cartesian coordinate system (x, y, z). We also assume no volume loss and no slip or detachment between the spherical body and the matrix during deformation. The basic equation has been already solved in different ways (e.g. Oertel 1965, Wakiya 1965, Masuda & Ando 1988a). Here we follow the method proposed by Masuda & Ando (1988a). Masuda & Ando analysed deflection of *simple shear* viscous flow around a spherical body. However, their basic equations can be also applied to *pure shear* viscous flow.

The method is briefly summarized as follows. The velocity vectors (u, v, w) are obtained by solving the Navier–Stokes equation for very slow flow:

$$\mu\nabla^2 u = \frac{\partial p}{\partial x}$$

$$\mu\nabla^2 v = \frac{\partial p}{\partial y} \tag{1}$$

$$\mu\nabla^2 w = \frac{\partial p}{\partial z}$$

and the continuity equation:

$$\frac{\partial u}{\partial x} + \frac{\partial v}{\partial y} + \frac{\partial w}{\partial z} = 0 \tag{2}$$

where μ is the viscosity, p is the pressure and ∇^2 is an operator identical to $\partial^2/\partial x^2 + \partial^2/\partial y^2 + \partial^2/\partial z^2$. Provided there is no rotation of the central sphere, the velocity u, v, and w, the solution of equations (1) and (2), are approximately expressed as

$$u = \sum_{n=1}^{24} A_{1,n} B_n$$

$$v = \sum_{n=1}^{24} A_{2,n} B_n \tag{3}$$

$$w = \sum_{n=1}^{24} A_{3,n} B_n$$

where $A_{1,n}$, $A_{2,n}$ and $A_{3,n}$ $(n = 1, 2, \ldots, 24)$ are functions of x, y and z and B_n $(n = 1, 2, \ldots, 24)$ are constants. The functions are fully described in Masuda & Ando (1988b), where the constants are determined to satisfy the boundary condition of the flow.

*Present address: Department of Earth Sciences, James Cook University of North Queensland, Townsville Q4811, Australia.

†Present address: Geology Division, CTI Engineering Co. Ltd, Nohonbashi Honcho, Tokyo 103, Japan.

Determination of the constants

The far-field velocity is assumed to be:

$$u = 0.2x$$
$$v = 0 \qquad (4)$$
$$w = -0.2z$$

which indicates that the deformation far from the sphere is plane strain, and that the compression and extension axes are parallel to the z and x axes, respectively. The determination of B_n ($n = 1, 2, \ldots, 24$) was performed as follows. We selected eight points far from the sphere where the flow is practically pure shear, and their velocities u, v and w were given by equation (4). Since $A_{1,n}$, $A_{2,n}$ and $A_{3,n}$ ($n = 1, 2, \ldots, 24$) are known, we derive a series of 24 equations whose unknown constants are B_n ($n = 1, 2, \ldots, 24$) by substituting (u, v, w) at the eight points into equation (3). B_n ($n = 1, 2, \ldots, 24$) are determined by solving these. Once a set of B_n ($n = 1, 2, \ldots, 24$) are determined u, v, w elsewhere can be calculated by equation (3).

RESULTS

Although the method is applied to three-dimensional flow, our analysis concentrates on the x–z plane where $y = 0$ because of simplicity. The particles on the x–z plane never leave this plane.

Velocity vector

The flow is highly affected by the existence of the sphere (Fig. 1). The effect is gradually attenuated with distance from the sphere until the flow becomes pure shear in regions far from the sphere. The velocity is very slow close to the sphere. The velocity vector is distributed symmetrically to the x and z axes.

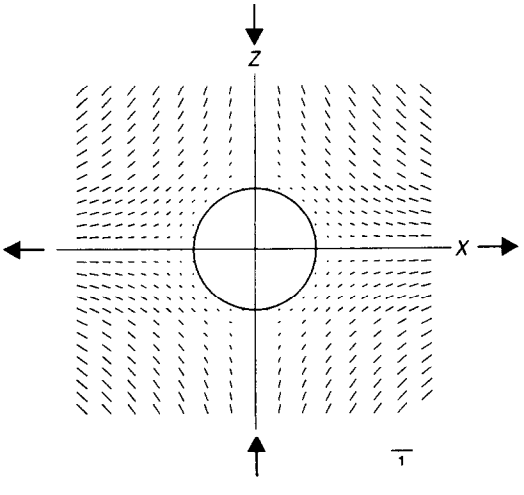

Fig. 1. Velocity vector field (m s^{-1}) around a rigid sphere. Bar lengths represent velocity magnitudes.

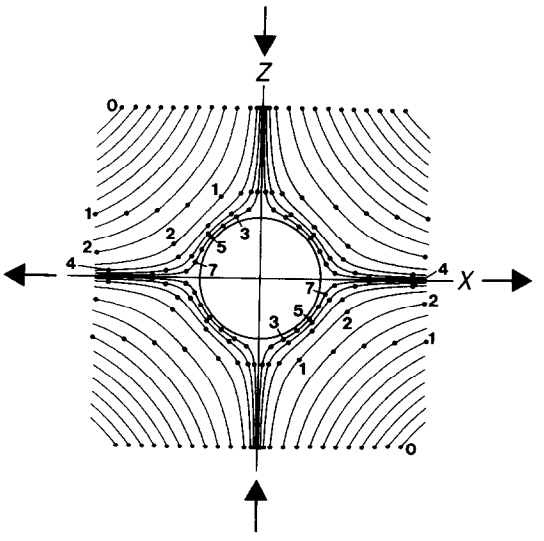

Fig. 2. Particle paths. The numbers attached to dots on each particle path indicate the magnitude of far-field compressional strain parallel to the z axis (ε) from the initial position at $z = 2.85$ and -2.85 ($\varepsilon = 0$).

Particle paths

Particle paths are traced by applying the same technique used in Masuda & Ando (1988a, p.341). Taking a particle of fluid at (x_i, z_i), the new position (x_{i+1}, z_{i+1}) of the particle after a short time (Δt) is approximately expressed as

$$x_{i+1} = x_i + u_i \, \Delta t$$
$$z_{i+1} = z_i + w_i \, \Delta t \qquad (5)$$

where u_i and w_i are u and w at (x_i, z_i), respectively. We can derive the next position of the particle in the same way. If Δt is very small, a smooth particle path is drawn. We set $\Delta t = 0.05$ in our calculation. The results are shown in Fig. 2. Each particle path is symmetrical to the x and z axes. Deflection of the flow is prominent in regions near the sphere (x and $z < 1.5$). As an indicator of strain, we use ε which is defined by the far-field compressional natural strain parallel to the z-axis. In practice, ε can be represented by the number of repetitions of the above calculation (number of strain increments). The numbers attached to dots on particle paths in Fig. 2 indicate ε values for the particles initially placed at $z = 2.85$ and -2.85. Slow velocity close to the sphere is accentuated by comparing these numbers.

Distortion of marker lines

Distortion of marker lines can be followed by applying the particle-path technique to initial particles arranged in a line (Fig. 3). The 'millipede structure' (Bell & Rubenach 1980) occurs when the lines were initially oriented at 90° to the x axis (i.e. parallel to shortening). Initially inclined lines (e.g. 45°) are *asymmetrically* distorted with respect to the x and z axes. If we do not know the reference coordinate axes and the type of deformation (simple shear or pure shear), we cannot distinguish lines of initial orientation of 70° at $\varepsilon = 1$ (Fig. 3)

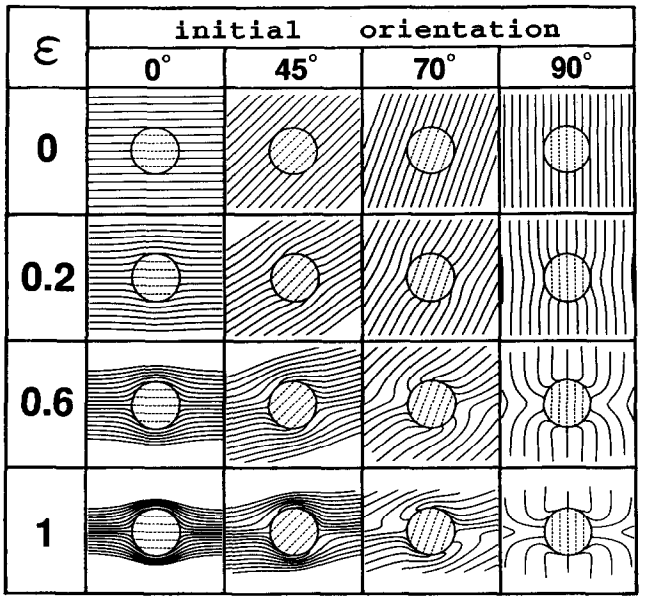

Fig. 3. Distortion of marker lines of various original orientation after various far-field compressional strains parallel to the z axis (ε).

from those of initial orientation of 135° at $\gamma = 2$ produced by simple shear (compare fig. 5 of Masuda & Ando 1988a).

Strain ellipses

Distortion of circles into strain ellipses (Fig. 4) is calculated using initial points arranged in circles. The longest axes of the strain ellipses are oriented symmetrically to the x and z axes. Figure 5 shows the distribution of strain schematically for $\varepsilon = 1.6$, from Fig. 4. Opposite regions very near the sphere and the x axis ($x < 1.1$) are least deformed, whereas those on the z axis ($z < 1.1$) are also least deformed. Opposite regions near the x axis ($|x| > 1.9$) are more deformed than those distant from the x axis.

Rate of strain

Components of rate-of-strain tensor (e_{xx}, e_{zz}, e_{zx}) (e.g. Masuda & Ando 1988a, p. 343) are expressed as:

$$e_{xx} = \frac{\partial u}{\partial x}$$

$$e_{zz} = \frac{\partial w}{\partial z} \qquad (6)$$

$$e_{zx} = \frac{1}{2}\left(\frac{\partial u}{\partial z} + \frac{\partial w}{\partial x}\right).$$

Thus, they are derived directly by differentiating u and w by x and z. Principal axes and principal strain are calculated easily from these components (e.g. Jaeger & Cook 1969, p. 13–14). The principal axes are shown in Fig. 6. Both their orientations and magnitudes are affected by the presence of the rigid sphere. Regions very close to the sphere ($\sqrt{x^2 + z^2} < 1.2$) appear highly deflected.

Pressure

Pressure p is directly obtained as a function of x, y and z by solving equations (1) and (2) (for detail, see Masuda & Ando 1988a). As a boundary condition, we assume $p = 0$ for the far-field. The magnitude of pressure is not obtained unless the viscosity of the matrix material is given. Here, we show normalized pressure (= pressure/viscosity) instead of pressure (Fig. 7). Pressure maximizes on the z-axis near the sphere, whereas it minimizes on the x-axis near the sphere. Apart from the sign, the pressure distribution pattern has an apparent 4-fold symmetry, a 2-fold one if the sign is taken into account. This pattern is very similar to that of simple shear (fig. 2

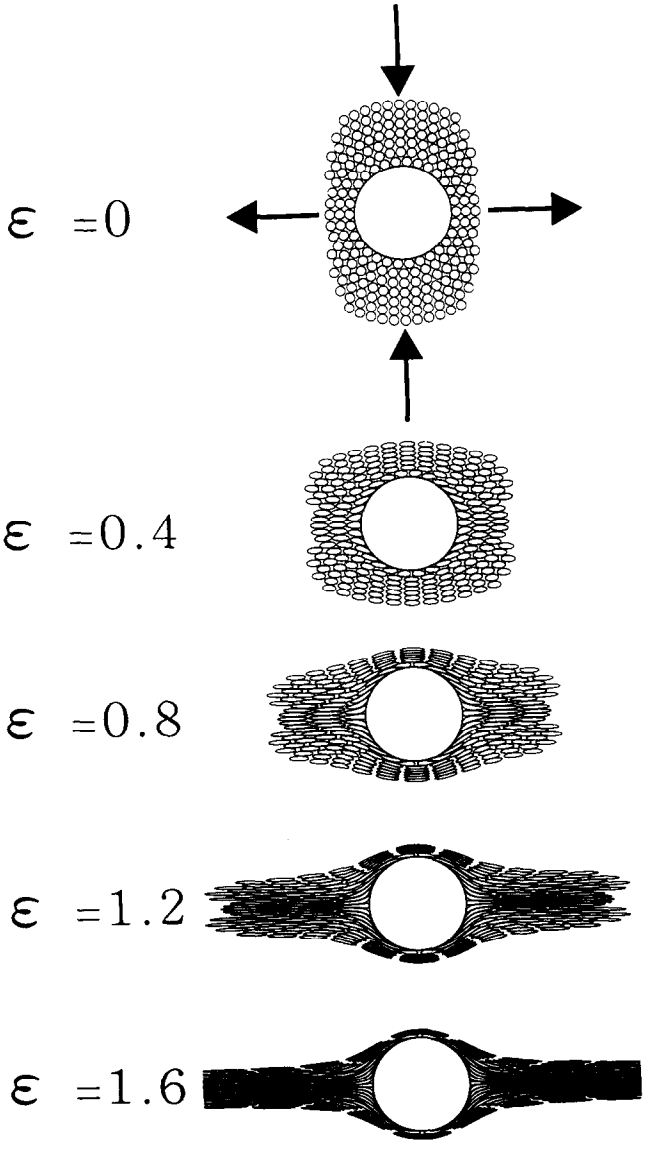

Fig. 4. Strain patterns and strain ellipses up to $\varepsilon = 1.6$.

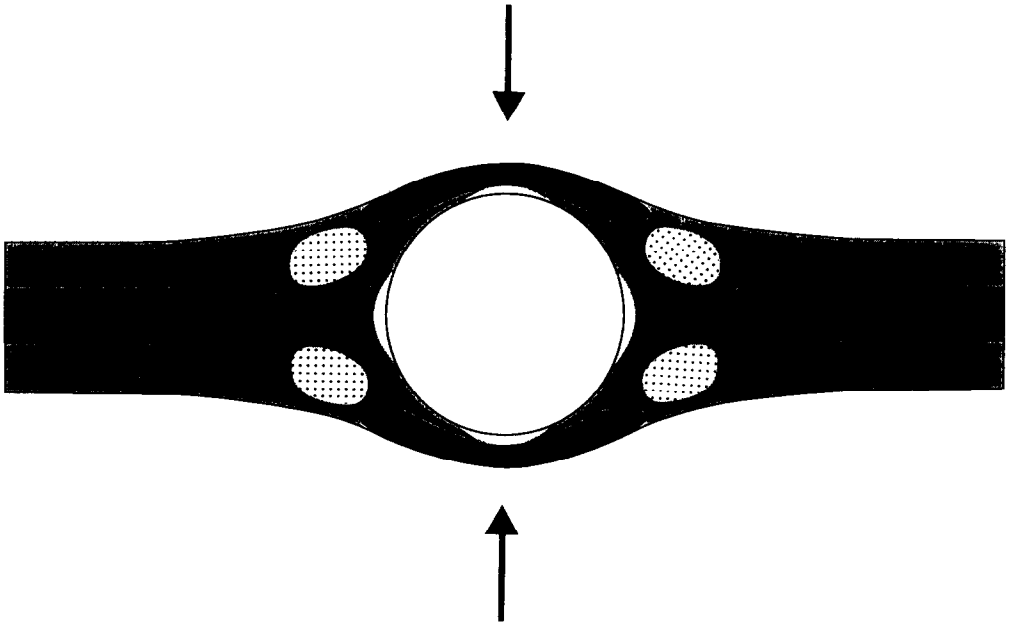

Fig. 5. Schematic drawing of the intensity of strain around the sphere at $\varepsilon = 1.6$. Regions in black, shaded, stippled and white have higher, equivalent, slightly lower and much lower axial ratios of strain ellipses than those at far field, respectively.

of Masuda & Ando 1988a) if the figure is rotated 45° counterclockwise.

Differential stress

Components of the stress tensor (σ_{xx}, σ_{zz}, σ_{xz}) (e.g. Lamb 1932, p. 574) are related to those of the strain tensor and pressure as

$$\begin{aligned} \sigma_{xx} &= -p + 2\mu e_{xx} \\ \sigma_{zz} &= -p + 2\mu e_{zz} \\ \sigma_{xz} &= 2\mu e_{xz}. \end{aligned} \tag{7}$$

As the magnitude of stress is not obtained unless viscosity is given, we calculated magnitude of normalized stress (stress/viscosity). The orientation and magnitude of principal stresses (σ_1, σ_3) are calculated from the stress components. Their distribution pattern is similar to that of the rate-of-strain tensor (Fig. 6) although the dimension is different, because a linear relationship between stress and strain is assumed for Newtonian viscous materials. The magnitude of differential stress $\sigma_1 - \sigma_3$ ($\sigma_1 > \sigma_3$) is obtained, as shown in Fig. 8. The pattern is symmetrical with the x and z axes. Approaching the sphere along the x and z axes, the differential stress first increases but then rapidly drops near the sphere (x or $z < 1.3$) and becomes zero at its surface. The differential stress maximizes on the sphere surface halfway between the axes, whereas it minimizes on the sphere and on the x and z axes. If no sphere is enclosed in the flow, the normalized differential stress is 0.8 everywhere, because we assumed a boundary condition of the flow as equation (4). As the normalized differential stress >1.6 is restricted to very narrow regions close to the sphere, extreme intensification of differential stress does not occur in most regions around the sphere.

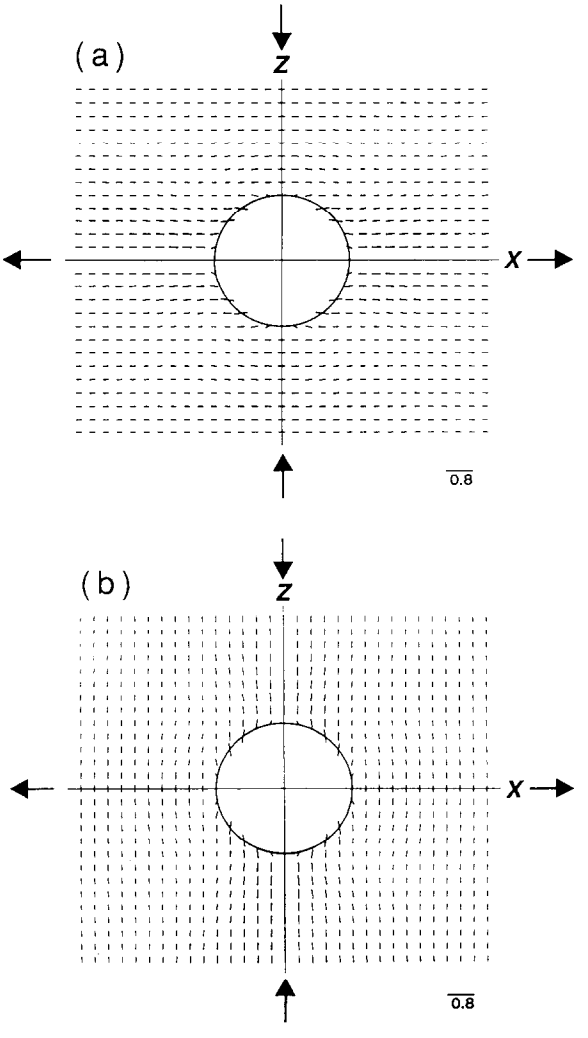

Fig. 6. Principal orientations of the rate-of-strain tensor (s^{-1}): (a) extensional; (b) compressional principal strain rates.

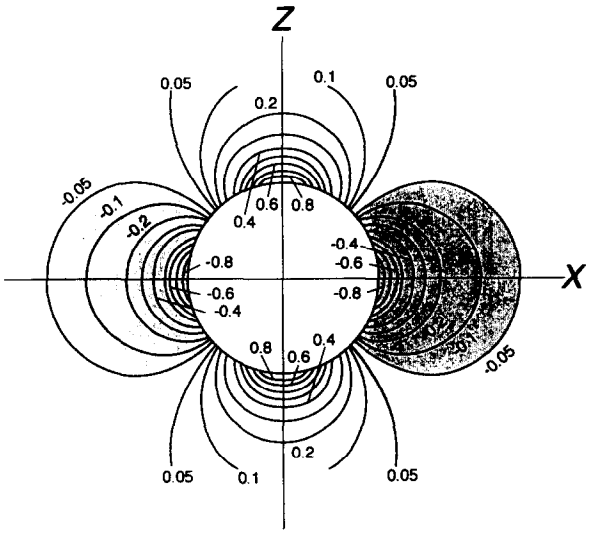

Fig. 7. Magnitude of normalized pressure (pressure/viscosity) (s^{-1}).

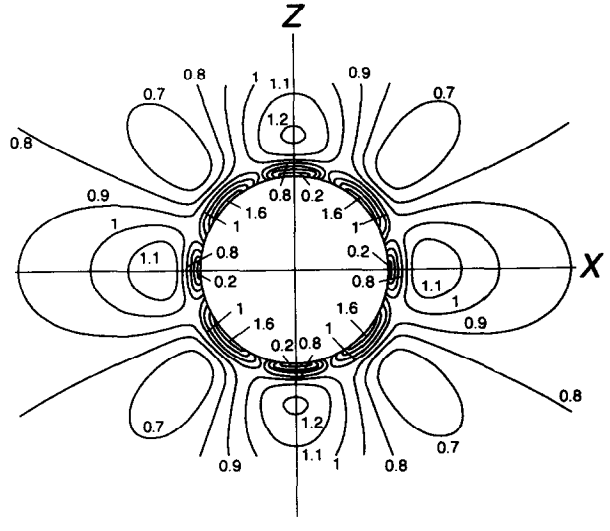

Fig. 8. Magnitude of normalized differential stress (differential stress/viscosity) (s^{-1}).

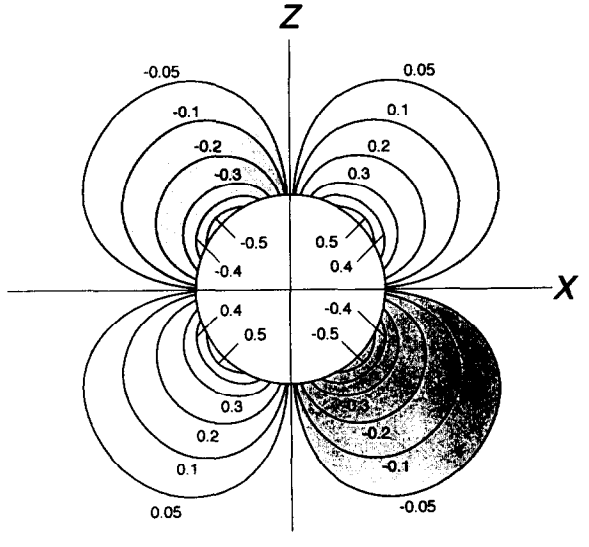

Fig. 9. Magnitude of vorticity (s^{-1}).

Vorticity

The vorticity (ω), defined as

$$\omega = \frac{\partial u}{\partial z} - \frac{\partial w}{\partial x},$$

is calculated directly by differentiating w and u by x and z in the same way as when we calculated components of strain tensor. The vorticity distribution is shown in Fig. 9 and is symmetrical to the axes apart from the sign. It becomes important only near the sphere. In the far field, vorticity asymptotically decreases to zero. Regions of large absolute vorticity (with positive and negative signs) correspond well to those with large differential stress (Fig. 8).

Kinematic vorticity number

Kinematic vorticity number, W_k (Means *et al.* 1980) is calculated by:

$$W_k = \frac{\omega}{\sqrt{2(s_1^2 + s_3^2)}}, \quad (8)$$

where s_1 and s_3 are the principal strain rates. The distribution of the kinematic vorticity number is shown in Fig. 10, and it is again symmetrical with the axes apart from the sign. The kinematic vorticity number is negative where the vorticity is negative. If no sphere is enclosed in the flow, the kinematic vorticity number would be zero everywhere.

GEOLOGICAL IMPLICATIONS

Our study assumes a *rigid sphere* in a *pure shear* deformation field. In rocks these might occur as porphyroclasts in mylonites, as porphyroblasts in metamorphic rocks, and in many other contexts. However, it is rather more difficult to judge whether the far-field deformation of such porphyroclasts or porphyroblasts was actually an ideal pure shear. Symmetrically deflected foliations wrapping around a central porphyroblast (Fig. 11a) may be the evidence of natural pure shear deformation.

A microstructure of the type schematically shown in Fig. 11(a) has been called a pressure shadow by Spry (1969). The pressure shadow is defined as 'a region in a rock which is protected from deformation by the presence of a relatively rigid object' (Spry 1969, p. 246). This definition relies on characteristics of the *strain* rather than the *pressure* distribution implied by its name. Accepting our assumptions made for the previous calculations, and comparing such a structure with the calculated distributions of pressure (Fig. 7), differential stress (Fig. 8) and strain (Fig. 4), we can state that the pressure shadow had developed in the 'shadow region' where pressure is low, but that the region is subject to a rather high differential stress and high strain, except for a narrow region very close to the sphere. Therefore, the

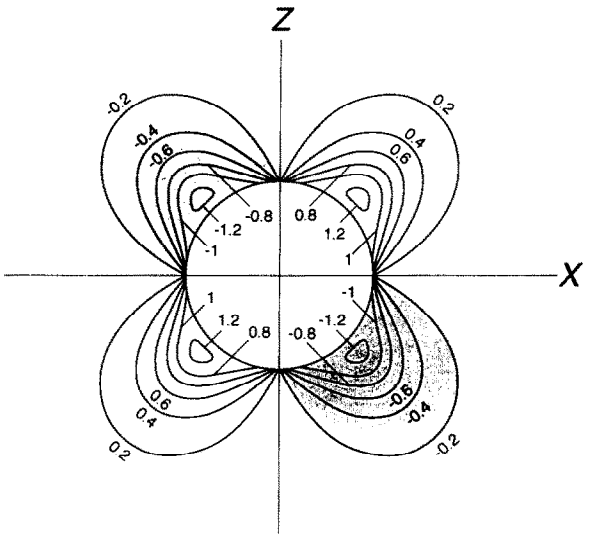

Fig. 10. Kinematic vorticity number.

definition and the concept of the pressure shadow should be revised as referring to pressure only and not to the strain and stress distributions. An alternative proposal is to abandon 'pressure shadow' and to compose a new name emphasizing the stress and strain distributions. However, this seems impractical, because the term 'pressure shadow' is in popular use.

The phenomenon sketched in Fig. 11(b) was called a 'pressure shadow' by Ramsay & Huber (1982), and a 'pressure fringe' by Spry (1969, p. 240). According to Ramsay & Huber (1982, p. 279), a 'pressure shadow' is defined as 'a region of low strain protected from deformation by a rigid or competent object in a rock of lower competence'. As this microstructure involves a competent matrix, the present results are not directly applicable. However, this definition is also not acceptable. The feature forms by detachment and subsequent separation between pyrite and the matrix and by the growth of fibrous minerals, such as quartz or calcite, in the gap. The detachment and separation are driven by the local tensile stress exceeding that in the surrounding material. Thus, the feature cannot be described or associated with 'a region of low stress'.

Acknowledgements—We thank S. Yoshida for critically reading the manuscript. We also thank S. H. Treagus, G. Oertel and M. Bjornerud for their constructive and helpful comments and for improving the English. The work was financially supported by the Ministry of Education, Japan.

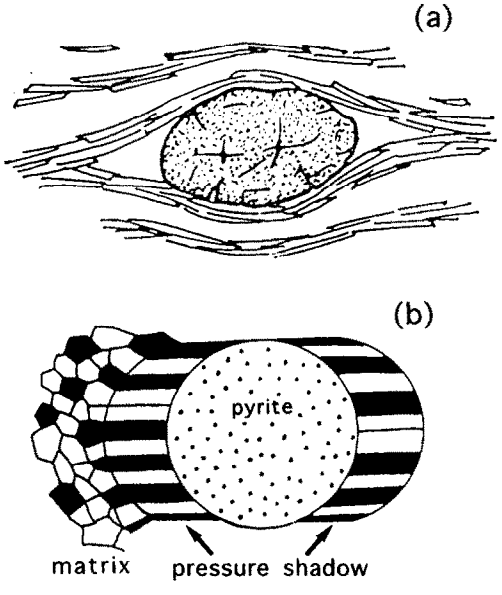

Fig. 11. (a) Porphyroblast and surroundings, re-drawn from Spry (1969, fig. 58(b), p. 252); (b) so-called pressure shadow near a pyrite grain, slightly modified from Ramsay & Huber (1982, fig. 14.7, p. 268).

REFERENCES

Bell, T. H. & Rubenach, M. J. 1980. Crenulation cleavage development—evidence for progressive bulk inhomogeneous shortening from 'millipede' microstructures in the Robertson River Metamorphics. *Tectonophysics* **68**, T9–T15.

Jaeger, J. C. & Cook, N. G. W. 1969. *Fundamentals of Rock Mechanics*. Chapman & Hall, London.

Masuda, T. & Ando, S. 1988a. Viscous flow around a rigid spherical body: a hydrodynamical approach. *Tectonophysics* **148**, 337–346.

Masuda, T. & Ando, S. 1988b. Viscous flow around a rigid spherical body: description of velocity vector field by a series of polynomials. *Geosci. Repts. Shizuoka Univ.* **14**, 85–88.

Means, W. D. 1976. *Stress and Strain*. Springer-Verlag, New York.

Means, W. D., Hobbs, B. E., Lister, G. S. & Williams, P. F. 1980. Vorticity and non-coaxiality in progressive deformation. *J. Struct. Geol.* **2**, 371–378.

Oertel, G. 1965. Slow viscous flow of an incompressible suspension. *J. Eng. Mech. Div. ASCE* **91**, 145–154.

Ramsay, J. G. & Huber, M. I. 1983. *The Technique of Modern Structural Geology. Vol.* 1: *Strain Analysis*. Academic Press, London.

Spry, A. 1969. *Metamorphic Textures*. Pergamon, Oxford.

Wakiya, S. 1956. Effect of a submerged object on a slow viscous flow: 2. A sphere in the flow between two parallel planes. *Res. Rep. Fac. Eng. Niigata Univ.* **5**, 1–12. (in Japanese).